Ultrafast Magnetization and Switching Dynamics

Theo Rasing, Hugo van den Berg, Thomas Gerrits, and Julius Hohlfeld

NSRIM Institute, University of Nijmegen
Toernooiveld 1, 6525 ED Nijmegen, The Netherlands
theoras@sci.kun.nl

Abstract. The development of femtosecond lasers has opened the way to creating external stimuli such as optical or magnetic field pulses that are much shorter than fundamental timescales such as spin–lattice relaxation or precession times and can be used to change the magnetization direction on an ultrafast timescale. In this chapter, two such approaches are discussed: precessional switching by exploiting specifically designed magnetic field pulses, generated by photoconductive switches, and ultrafast thermomagnetic writing using femtosecond lasers in combination with an external static field. Consequences for applications in magnetic storage (MRAM and MO recording) are discussed.

"How fast can the magnetization of a magnetic medium or element be changed" or "what are the fundamental and practical limits of the speed of magnetic writing and reading"?

The answers to these questions will have far reaching consequences for the future of data storage and retrieval, topics that are connected to large commercial markets. Moreover, asking these questions is connected with a lot of exciting research that addresses, very fundamental issues of spin- and magnetization dynamics as well as very practical points of how to generate and detect the magnetization dynamics of interest.

Traditionally, magnetization dynamics was studied under quasi-equilibrium conditions and thought of as a rather slow process, limited to the nanosecond regime [1] by domain-wall motion and spin–lattice relaxation time. The development of femtosecond (fs) laser sources has opened the way to creating external stimuli (optical, field, or current pulses) that are much shorter than the fundamental timescales such as spin–lattice relaxation times and precession times. The use of these short stimuli allows us to study magnetization dynamics for real nonequilibrium conditions and has already led to exciting results demonstrating ultrafast changes in magnetization on picosecond timescales.

Optical excitation of ferromagnetic systems with ultrashort laser pulses leads to the heating of electrons far above equilibrium and consequently can lead to the reduction or even erasure of magnetization M within very short times. Though great care should be taken to separate real magnetization dynamics from optical artifacts due to spin-independent changes in elec-

B. Hillebrands, K. Ounadjela (Eds.): Spin Dynamics in Confined Magnetic Structures II,
Topics Appl. Phys. **87**, 213–251 (2003)

tron distribution, time-resolved (pump-probe) linear and nonlinear magneto-optical experiments have clearly demonstrated the collapse of M within less than 2 ps in itinerant ferromagnets [2,3,4,5,6,7]. These experimental results demonstrate unambiguously that the traditional point of view has to be revised. However, until today there is no microscopic theory reported in the literature that can explain all experimental results consistently.

In addition to the variations in the magnitude of M with time, optical excitation can also lead to coherent precession of the magnetization direction. The latter was attempted in a clever approach by *Ju* et al. [8], who used a femtosecond laser pulse to reduce the antiferromagnetic coupling in an exchange-coupled FM/AF bilayer, thereby indeed inducing ultrafast magnetization rotation. Similar, but less pronounced precession dynamics was also observed by *Koopmans* et al. in a thin nickel film and explained by temperature-dependent variations in the anisotropy field [7]. A rather unique approach was developed by *Siegmann* et al. [9] who used a short (picosecond) current pulse to induce precessional switching. This required, however, quite a special current source, namely the Stanford Linear Accelerator, which rather limits the general applicability of this approach.

Despite the large number of publications on ultrafast magnetization dynamics, only a few reports address the technologically relevant process of magnetization reversal. It is obvious that for true rotation or reversal of magnetization, simply heating the electron system above the Curie temperature is not sufficient. However, in combination with either a static or pulsed magnetic field, optical excitation by femtosecond laser pulses induces magnetization reversal that can be extremely fast [12]. Recent experiments also showed generation of ultrashort field pulses in a Schottky diode [10]. An alternative approach is using a short magnetic field pulse that, by exerting a torque on magnetization M, leads to subsequent precession of M [13]. In principle, one should be able to switch M at a maximum rate of half the precessional frequency (typically 10–1000 ps), if not for the fact that the damping of this precession is usually very slow (in the nanosecond regime). Therefore, precessional switching faces two challenges: generation of short magnetic field pulses (much shorter that the inverse of the precessional frequency) and suppression of the precession (or ringing) at the proper time.

In the past 3 years, we have developed some strategies in Nijmegen to address these issues of magnetization reversal by exploiting combinations of femtosecond laser excitation with static magnetic fields and generating ultrashort magnetic field pulse using photoconductive switches excited by femtosecond laser pulses. In both cases, we have been able to obtain very fast real switching of the magnetization of the magnetic elements of interest, though using very different mechanisms – precessional switching and femtosecond laser-pulse-induced reversal. In precessional switching by short magnetic field pulses, we have obtained a solution to the "ringing" problem [25,26], not by increasing the damping but by "designing" proper magnetic field pulse that

stop the precession at the desired moment, i.e., at half the precessional period. For femtosecond laser-pulse-induced reversal, which is basically nothing other than thermomagnetic writing using femtosecond lasers, we were able to accelerate the speed of the writing process tremendously, i.e., the reversal of the magnetic bit, by increasing the laser fluence.

In this chapter, we will address switching by magnetic field pulses as well as laser-induced reversal in the presence of a magnetic field. In both cases, we will start with a brief introduction of the basic phenomena, describe the experimental approach, and follow with a discussion of the results obtained. Finally, an outlook for future development will be given. For more extensive introductions to some of the topics relevant to this chapter, we refer readers to the preceding book in this series [14].

1 Switching by Short Magnetic Field Pulses

Field-induced magnetization dynamics has already been studied for more than half a century [15]. The theoretical description goes back to the phenomenological precession equation formulated by Landau and Lifshitz in 1935.

1.1 Precessional Dynamics

Including the phenomenological damping constant α leads to the so-called Landau–Lifshitz–Gilbert (LLG) equation of magnetization motion for small α:

$$\frac{\mathrm{d}\boldsymbol{M}}{\mathrm{d}t} = -|\gamma|\mu_0 \cdot (\boldsymbol{M} \times \boldsymbol{H}_{\mathrm{eff}}) + \frac{\alpha}{M_s} \cdot \left(\boldsymbol{M} \times \frac{\mathrm{d}\boldsymbol{M}}{\mathrm{d}t}\right) \tag{1}$$

The first term describes the precessional motion where γ is the gyromagnetic ratio given by $g\mu_{\mathrm{B}}/h$; g and μ_{B} are the spectroscopic splitting factor and the Bohr magneton, respectively. The second term describes damping, using the phenomenological (Gilbert) damping constant α. Magnetic motion is driven by the total effective field, $\boldsymbol{H}_{\mathrm{eff}}$, that includes the external bias field, the fields due to anisotropy, and the applied pulse field. Typical numbers for γ and α for Permalloy are $\gamma = 17.6 \times 10^7/\mathrm{Gs}$ and $\alpha = 0.01$, leading to precession frequencies of the order of several GHz and damping times of the order of nanoseconds. These values imply that magnetic field pulses with typical rise times or delay times in the 10-ps range are required to trace the "true" intrinsic magnetic response of magnetic Permalloy elements unaffected by external field pulses.

Regardingprecessional switching, it is important to note that magnetization always precesses about the direction of the effective field. Therefore, precessional reversal of a magnetic bit is possible only by effective fields that have at least an infinitesimal component opposite and a component perpendicular

to the initial M. In addition, demagnetization in thin films significantly increases the speed of bit reversal. In an infinitely thin film, the demagnetizing field is exclusively given by the polar component of M and is generally much larger than the applied bias field and pulse field. The demagnetizing field is the driving force for ultrafast reversal of a single bit by precessional motion because it gives rise to torque for the in-plane motion of M. In summary, a large effective field component perpendicular to M is necessary for ultrafast switching. This can be achieved by short rise-time and high-peak field pulses of appropriate length.

Weak excitations, for which the magnetization component along the bias field remains almost constant, lead to small M components normal to the film plane, and the tip of the magnetization vector describes an elliptical orbit about the equilibrium state for a static equilibrium state and zero damping. For field pulses with strengths much larger than the bias field, the component of M along the bias field also changes strongly, and the demagnetization fields may even be so strong that the magnetization reverses.

Numerical solutions of the LLG equation that illustrate magnetic motion for weak and strong excitations are shown in Fig. 1. The simulations are carried out for a typical field pulse, used in the present experiments, with a rise time of 10 ps and a decay time of 400 ps. (More extended simulations can be found in the chapter by Russek et al.)

Investigations of the magnetization dynamics following weak excitation are useful for obtaining information about sample properties, like damping constants and anisotropies. This information can then be used to estimate the proper experimental conditions for strong excitation experiments that will lead to precessional switching. As mentioned earlier, the possibility of

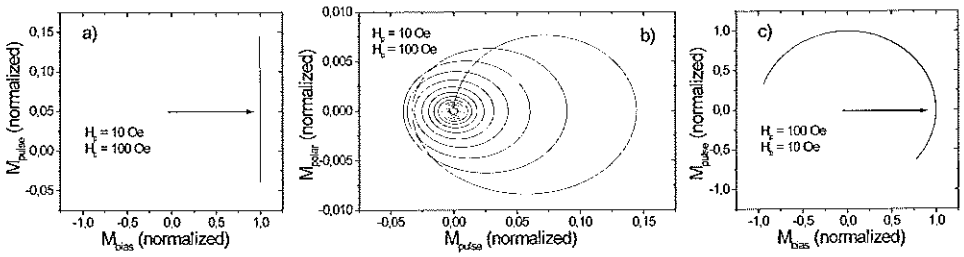

Fig. 1. Simulations of the precessional motion of M for weak (a,b) and strong (c) pulse excitation. (a) The projection in the thin-film plane. It can be seen clearly that the motion of M can be linearized for small angle excitations because M_{bias} does not change. The motion then is elliptical, as shown in (b), where the projection in the plane perpendicular to the thin film and parallel to the field pulse is shown. The in-plane projection of M for a strong pulse excitation is given in (c). M follows a circular path because the polar component of M is small due to large demagnetization fields. The *arrows* in the figure show the initial magnetization state

generating ultrashort magnetic field pulses is one of the most important prerequisites for corresponding measurements and will be discussed in the following.

1.2 Generation of Field Pulses using Photoconductive Switches

To generate short magnetic field pulses, we use so called photoconductive Auston switches, triggered by a femtosecond optical laser pulse that generates a current transient in a coplanar wave guide. This approach, well known for electro-optic sampling, was first exploited by *Freeman* et al. to generate picosecond magnetic field pulses [16].

We use the direct gap semiconductor GaAs as a photoconducting material because its band gap is extremely well fitted for excitation by a Ti:sapphire laser. A bias voltage is applied to the two copper electrodes that are structured into a coplanar waveguide. While illuminating the gap between the electrodes, an electrical pulse is generated and travels through the waveguide. The rise time of the electrical pulse at the gap depends on the capacitance, the inductance, and the resistance of the gap [17]. While traveling through the waveguide, dispersion and attenuation of the terahertz pulse is observed [18]. The decay time of the pulse is determined by the carrier lifetime of the material. Undoped GaAs has typical lifetimes of 100–500 ps, whereas low-temperature-grown GaAs may have lifetimes of a few picoseconds [19].

Figure 2a is a photograph of the two Auston switches that are attached to our waveguide structure. Each switch consists of a finger structure, which enlarges the area for the excitation of carriers and thus the total current. The gap between the electrodes is 15 μm. As the pump-laser beam hits the device at a certain angle, the electrodes would shade some area within the photoswitch, which would decrease the generated current. Our finger structure is

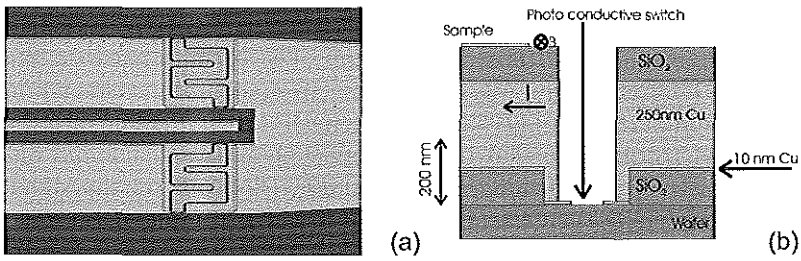

Fig. 2. (a) Photograph of photoswitches. Another electrode can be seen between the finger structure. This is a thin copper electrode that should prevent shadow effects from the larger electrodes. (b) Cross section of the device. The 100-fs laser pulses pump carriers across the gap within the finger electrodes. A current pulse is coupled into the waveguide and passes the sample, while inducing an in-plane magnetic field. The 10-nm copper layer is used to overcome shadow effects due to the thick electrodes [27]

designed so that at the edges of the thick electrodes, 10-nm thin electrodes are present, which are separated by 5 μm from each other. Because the thickness of the electrodes chosen is smaller than the skin depth of the incoming laser beam, light can travel through and excite carriers beneath. So no resistance due to dark areas within the switch is present. This technique allows us to vary the angle of incidence of the pump beam without changing the resistance of the photoswitch.

A cross section of our device is shown in Fig. 2b. The copper electrode consists of a thick 250-nm layer and a thin 10-nm layer. The magnetic element is normally deposited on top of the electrode but is isolated from it by a thin SiO_2 layer. An insulating layer of SiO_2 deposited beneath the copper electrodes ensures that the electrodes are insulated from each other. No leakage current can flow from the signal line to the waveguide ground flats through the wafer. Only the photoswitches are kept free. As a substrate, we used undoped GaAs. Large currents and small signal lines are needed to generate large magnetic fields on the signal line. Large currents require large photoswitches because the total current I generated in a photoswitch and sent through the waveguide depends on the carrier density times the area of the photoswitch. Small signal lines lead to large current densities and thereby to large magnetic fields. The magnetic field close to the surface of the signal line is given by $H = I/2w$, where I is the current and w the width of the signal line.

Figure 3 is a photograph of the complete waveguide structure. The two photoswitches with dimensions of 65 μm × 65 μm (*white arrows*) are rather big in comparison to the signal line, which is only 10 μm wide (*black arrow*). A tapered connection between the signal line and the switches takes care of charge transfer. The design of the waveguide is based on a model [18,20] for propagating current pulse on a signal line that describes the attenuation and dispersion due to the surface impedance of a coplanar strip line, including the dielectrics surrounding it. We chose the dimensions of the signal line so that 0.01–1 THz pulses would have the lowest possible attenuation and dispersion. The width of the signal line chosen was 10 μm. The spacing between the signal line and the ground flats was also 10 μm. To squeeze the current into the signal line without reflections, the ratio between the middle line and the spacing was kept constant, so that the impedance of the waveguide did not vary [18,20]. A change in impedance would cause reflections on the signal line, thereby broadening the current pulse and lowering the maximum field obtainable.

The purpose of the second photoswitch will be elucidated in Sect. 3 on field-pulse shaping. For the experiment presented in this section, both switches are excited simultaneously and act as one single switch.

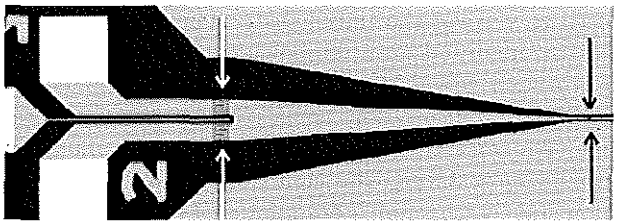

Fig. 3. A photograph of the waveguide used in the experiment. The taper concentrates the current onto the 10-mum signal line. A thin 10×20 μm Permalloy film is placed at the end of the taper. Two big ground flats are placed around the signal line as a waveguide [27]

1.3 The Experimental Setup

A stroboscopic femtosecond time-resolved pump-probe technique is applied to follow the precessional dynamics induced by a short magnetic field pulse within the first nanoseconds; the corresponding experimental setup is shown in Fig. 4. We use 100-fs, 800-nm pulses generated at a repetition rate of 76 MHz by a Ti:Sapphire laser for our measurements on magnetic thin films. The laser is sent to a BK7 beam splitter, which divides the beam into two parts – a pump beam and a probe beam. The pump beam is used to excite the photoswitch. The probe beam detects the magnetization state of the magnetic element. The time delay between probe and pump beam is used for scanning the magnetic response in the time domain stroboscopically, at

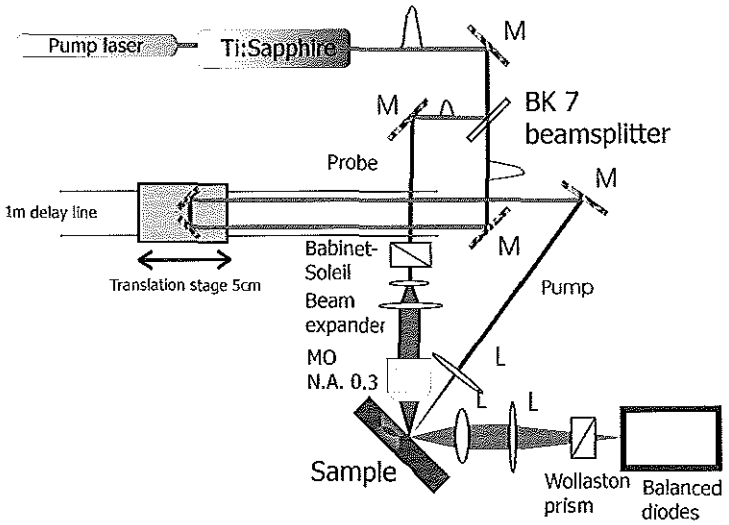

Fig. 4. The experimental setup for time-resolved pump-probe MOKE experiments [27]

which the bias field is used to recover the initial state. The pump beam is brought onto a retroreflector, mounted on a 50-mm long translation stage. This translation stage has a step width of 1 micron, which corresponds to a pump-beam time delay of ≈ 7 fs in air. The translation stage is mounted onto a 1-m long delay line. We can move the translation stage on the delay line with an accuracy of 0.5 mm $\approx$ 3.3 ps. The combination of a long delay line and a short translation stage with small steps allows us to measure both nanosecond and femtosecond dynamics. (To improve our system further, we recently replaced this combined delay line by a new, fully motorized delay line of 500 mm.) Returning from the retroreflector, the pump beam is directed by another mirror to the device, where it is focused at normal incidence onto the photoswitch.

The probe beam travels to a Babinet–Soleil compensator, which is used to change the polarization of the beam. After the Babinet–Soleil compensator, the probe beam is expanded by a factor of 5 and subsequently focused by a long-working-distance microscope objective (N.A. 0.3) to a spot size of at least 5 μm on the magnetic film. The use of a long-working-distance objective was necessary to avoid screening the pump beam.

The whole setup is designed so that we can probe the magnetization at an angle of incidence of 45° as well as at normal incidence. Thus, we can individually probe the polar effect at normal incidence, whereas mixing of the longitudinal and polar effect is seen at 45°. The 45° configuration also allows us to detect the in-plane magnetization components by magnetization-induced second-harmonic generation (MSHG) [23] (see also Sect. 3). Figure 5 is a schematic drawing of the time-resolved MOKE measurement. A longitudinal magnetic bias field is applied to the sample. The pump beam is chopped

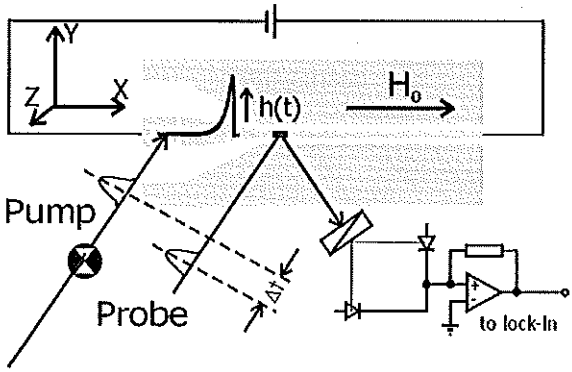

Fig. 5. Scheme of the setup of the time-resolved MOKE experiment and single field-pulse excitation. The 100-fs pump pulse excites a current pulse, which is concentrated in the taper and launched into the signal line. The response of the magnetic element to the related field pulse, $h(t)$, is measured by detecting the Kerr rotation of the 100-fs probe pulse as a function of the pump-probe delay Δt [27]

and activates the photoswitch. With the probe beam, we measured the linear MOKE signal by using the balancing diodes and lock-in technique [16]. While delaying the pump beam, we can get temporal information about the magnetic system due to the short magnetic field pulse.

1.4 Field-induced Precession Dynamics

In this section, we will discuss the precession dynamics obtained for weak excitation by a single field signal. The sample was a 16-nm NiFe (81 : 19) film, fabricated by magnetron sputtering and located on top of the signal line (the middle electrode of the waveguide). Its lateral dimensions are $10 \times 20\,\mu m$ and it is covered with a 3-nm Cr layer to prevent corrosion. The Permalloy elements are small in comparison to the signal line width and are located in the middle and close to its surface to ensure that the field is homogeneous and in-plane inside the element.

The magnetic response of the NiFe film that is induced by the in-plane field of 9 Oe along the y axis perpendicular to the in-plane bias field of 94 Oe in the x direction was investigated by time-resolved detection of the Kerr rotation (see Fig. 5). For the present large bias fields and weak excitations, the change in the longitudinal M_x component is small, and therefore the contributing longitudinal Kerr signal due to a change in M_x can be neglected compared to the polar Kerr signal. Thus, the corresponding data in Fig. 6 shows the z component of magnetization precession.

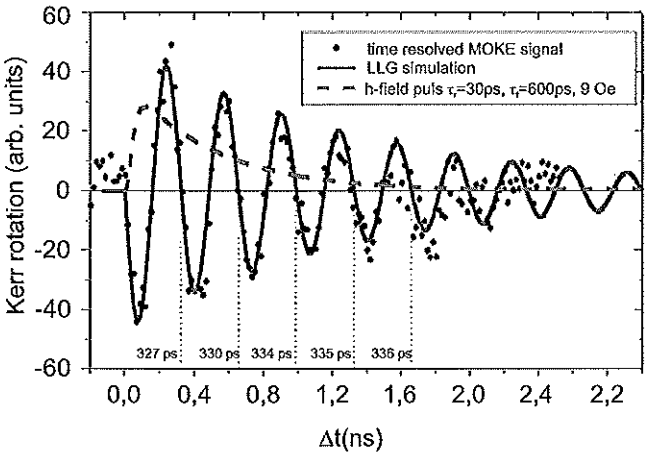

Fig. 6. Precession of the ferromagnetic NiFe system, as measured by a time-resolved pump-probe MOKE experiment in the 45° configuration. The bias field for this measurement was 94 Oe. The *solid line* shows the LLG simulation for the given system. The *dashed line* shows the shape of the magnetic field pulse derived from this simulation [27]

A stronger effective field causes an increase in the precessional frequency [see (1) and (3)], so the observed asymptotic decrease of the precession frequency toward a lowest value can be attributed to the decay of the field-pulse amplitude (*dashed line*). The asymptotic value is then determined by the bias field and the anisotropy of the film element. After the signal field has vanished, the x axis of the system constitutes the central axis of precession.

The shape of the magnetic field can be derived from these data via fits based on the LLG equation and can be described by

$$h(t) = h_0 \cdot \left(1 - \mathrm{e}^{-t/\tau_\mathrm{r}}\right)^3 \mathrm{e}^{-t/\tau_\mathrm{f}}, \tag{2}$$

where h_0 is the maximum field-pulse amplitude, τ_r is the rise time, and τ_f denotes the decay time of the pulse. By fitting this pulse to the change in precessional frequency in time, we obtained $h_0 = (9 \pm 1)\,\mathrm{Oe}$ and $\tau_\mathrm{f} = (600 \pm 100)\,\mathrm{ps}$. For the rise time of the pulse, we could only determine a lower and upper limit of 10 ps and 60 ps, respectively. The fit also provided the saturation magnetization of the film, and the corresponding value of $M_\mathrm{s} = (800 \pm 20)\,\mathrm{emu/cm^3}$ confirmed by the results of additional Vibrating Sample Magnetometer (VSM) measurements. For the simulation presented in this part, we used a 9-Oe field pulse with a rise time of 30 ps and a decay time of 600 ps. A more precise characterization could have been achieved by direct sampling of the field-pulse shape by a time-resolved magneto-optical method [16] or by directly probing the current pulse by using a photoconductive sampling technique with a picosecond Scanning Tunneling Microscope (STM) [22].

For small excitation, the precessional frequency ω is given by the determinant of the coupled system of differential equations. For bias fields that are large compared to the field-pulse amplitude, however, one can assume that M_x remains constant and equal to the saturation magnetization M_s and obtain the following analytical approximation for the resonance:

$$\omega^2 = \gamma^2 \cdot (H_\mathrm{b} + 4\pi M_\mathrm{s} + H_{\mathrm{s}x})(H_\mathrm{b} + H_{\mathrm{s}x}). \tag{3}$$

Here, $H_{\mathrm{s}x}$ represents an effective field in the x direction that includes the sum of the induced and the in-plane magnetostatic anisotropy of the thin-film element. H_b is the applied bias field. $H_{\mathrm{s}x}$ was determined by measuring the hard-axis hysteresis loop of the element that could be well described by two uniaxial anisotropic constants for a second-order anisotropy $K_1 = 5.2 \times 10^3\,\mathrm{erg/cm^3}$ and $K_2 = -3.0 \times 10^3\,\mathrm{erg/cm^3}$, yielding an effective anisotropy field of 2 Oe along the long axis of our element for small excursions from the equilibrium state. This field is small compared to the in-plane magnetostatic anisotropy field, which can be accessed for the central region of a rectangular film. We calculated the demagnetization factors: $N_x = 0.0002$; $N_y = 0.0009$; $N_z = 0.9989$. This gives a magnetostatic anisotropy field of $4\pi M_\mathrm{s}[N_y - N_x] = 7\,\mathrm{Oe}$. Because K_1 and K_2 represent all anisotropies due to the properties of the element, we can conclude that except for magnetostatic anisotropy, other anisotropic

effects, such as field-induced anisotropy and magnetoelastic anisotropy at the edges of the thin film, play a dominant role.

Figure 7 shows the bias field dependence of the precessional frequency. From (3), it follows that the square of the precessional frequency depends linearly on the applied bias field and that the anisotropy field of the film element can be determined for $\omega = 0$. We plotted this dependence, with $M_s = 800\,\mathrm{emu/cm^3}$ and $H_{sx} = 2\,\mathrm{Oe}$, and got good agreement with the measured data (see solid line in Fig. 7).

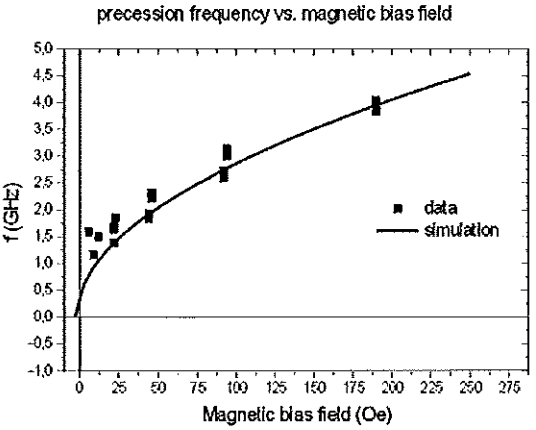

Fig. 7. Observed precessional frequency $f(= \omega/2\pi)$ as function of the magnetic bias field H_b, showing $f^2 \propto H_b$ in accordance with (3)[27]

2 Coherent Magnetization Reversal by Field-Pulse Shaping

Coherent magnetization reversal of thin-film magnetic elements can be induced by in-plane field pulses when the magnetization is pulled out of the plane so that the effective field is almost along the surface normal and the precession is confined to the film plane (see Fig. 1b). This can be accomplished by strong excitations, i.e., when the amplitude of the applied field pulse is much larger than the bias field. To reverse the magnetization in the shortest time given by half the precessional period, one should stop the precessional motion at exactly that moment. This can be achieved either by tuning the damping of the ferromagnetic system to the critical value [17] or by controlling the shape of the magnetic excitation pulse (see also the contribution of *Russek* et al. in this book). Because the reversal time for critical damping is longer than the period of underdamped magnetization precession, we will concentrate on the possibility of taming a ferromagnetic system by controlling the magnetic

excitation pulse length, as shown before by the *Hillebrands* group and the *Silva* group just below the nanosecond regime [25,26]. By superimposing two independently triggered magnetic field-pulse sources as described above, we can modify field-pulse shapes on a picosecond timescale. By modifying the amplitude and duration of the applied field pulse, the course of the torque $M \times H$ exerted on the magnetization and thus the magnetic motion can be controlled. Stopping this motion is of primary interest in ultrafast switching. It can be achieved by aligning H_{eff} parallel to M while M passes an energetic minimum, so that the torque acting on the magnetization becomes zero.

2.1 Experimental Approach for Pulse Shaping

The experimental technique for generating shaped magnetic field pulses of varying width, amplitude, and strength is based on using two independent photoconductive switches integrated in the waveguide. As discussed in Sect. 4, the trailing edge of the current burst of one single switch is characterized by exponential decay, dominated only by one time constant. This fact can be exploited for generating field pulses with varying pulse widths by superimposing the signals of two switches. Experimentally, this means that we use a pump-pump probe scheme with two independently controlled pump pulses that together generate the required magnetic field pulse to excite the magnetic element. Figure 8 shows schematically that due to the exponential character of the photoconductive response, the total current can be canceled at the trailing edge of the second (quenching) field burst by adapting its strength.

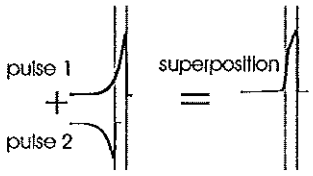

Fig. 8. Principle of magnetic field pulse cancelation due to the exponential character of the trailing edge

2.1.1 Pump-Pump-Probe Setup

A schematic drawing of the waveguide structure designed to launch two independent current pulses down the signal line is shown in Fig. 9 (a photograph of the actual switches can be seen in Fig. 2). As schematically shown in the figure, the two photoswitches are excited by two independent femtosecond laser pulses – pump-pulse 1 (excitation pulse) and pump-pulse 2 (quenching pulse). Adjustment of the two voltages at the source electrodes and of the mutual time delay between the excitation of the switches opens the way to varying the width of the magnetic field pulses. In particular, generation of

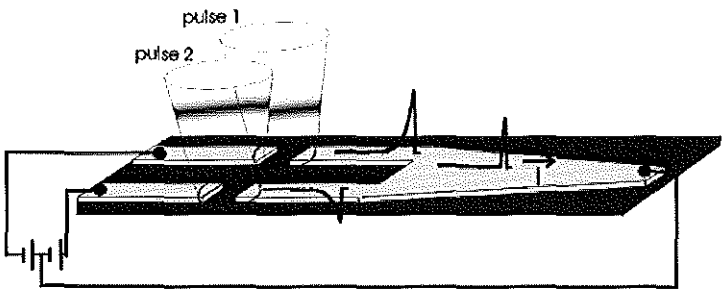

Fig. 9. Schematic drawing of the double photoswitch setup that allows one to control the shape of the field pulses generated [28]

magnetic field pulses that are limited only by the rise time ($\approx$ 10 ps) and not by the decay time ($\approx$ 600 ps) of the photoconductive switches is possible by choosing the right combination of voltages with opposite polarity at the source electrodes. Voltages up to ± 30 V could be applied and the usual peak power of the laser pulse excitation is 100 MW/cm^2. The optical pump and probe pulses are generated by splitting one single laser pulse, so the magnetic field is perfectly synchronized to the probe pulse. The jitter induced by changes in optical paths is negligible compared to the width of the laser pulse, so that extremely high temporal resolution is achievable. Thus, well-defined magnetic field pulses of 100 Oe, of duration less than 50 ps, and a jitter considerably better than 1 ps can be generated.

The experimental setup is shown in Fig. 10 and is similar to that used in Sect. 3. After the delay line DL1, the pump beam is split at a 50:50

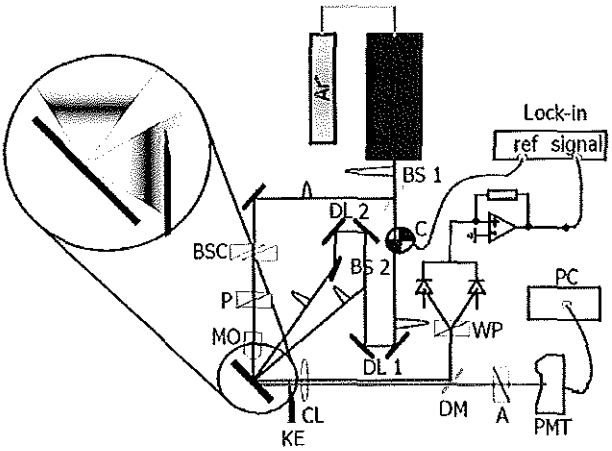

Fig. 10. Schematic experimental setup for pump-pump probe experiments, allowing us to generate shaped in-plane magnetic field pulses and 3 d probing of the induced magnetization dynamics [30]

beam splitter (BS2) into two equal pump-laser pulses. The transmitted part is directed to a second 100-mm delay line (DL2) that is used to adjust the delay between the two pump pulses. Proper adjustment of the strength of the current pulses is achieved by adapting the voltages at the switches of the source electrodes.

2.1.2 Three-Dimensional Probing of M

The three individual components of M are measured by using polar MOKE and longitudinal as well as transversal MSHG [34,35]. Three independent successive measurements of the complete response of the magnetic system have been done to reconstruct the 3 d trajectory of the magnetization vector. For the polar MOKE, the incident beam should be perpendicular to the surface to prevent any contribution of the longitudinal component of M to the signal obtained. Using the numerical aperture of the MO and a knife-edge (KE) to block all large-angle photons, the longitudinal contribution is sufficiently reduced because the incoming photons are nearly at normal incidence, whereas the sample is at 45° with respect to the optical axis of the incident beam (see Fig. 10). The light is collimated by a collimation lens (CL) and directed to a dichroic mirror, where the fundamental 800-nm pulse is reflected onto a Wollaston prism (WP) and equally split onto two photodiodes. The difference signal of the two photodiodes is put into a lock-in amplifier with the modulation frequency of the chopped pump beam (C) as a reference. The MSHG is measured after transmission through the dichroic mirror and without the knife-edge in front of the collimation lens. An analyzer is used to separate the measurement for the two in-plane (xy) components of M. The longitudinal component is measured by detecting the s-polarized second-harmonic yield that is generated by the p-polarized fundamental ($p_{\text{in}} - s_{\text{out}}$). The transversal component is measured via the $p_{\text{in}} - p_{\text{out}}$ polarization combination. The second-harmonic yield was measured by a photomultiplier tube (PMT) in combination with a photon counter (PC). As recently shown by *Kabos* et al. [33], it is also possible to measure the in-plane components simultaneously; however, we preferred to measure these components separately because the analysis is easier.

2.2 Excitation by Shaped Magnetic Field Pulses

2.2.1 Pulse Width Controlled Excitation

The data presented in Fig. 11 show the individual response due to individual field pulses and also their combined effect, as observed by polar MOKE. The *open squares* correspond to the signal from excitation by the first switch at which a positive voltage is applied. The *open triangles* represent the pulse from the second switch – the quenching pulse for the first pulse. The two excitations are separated by 180 ps, and their amplitudes were 25 Oe and −20 Oe,

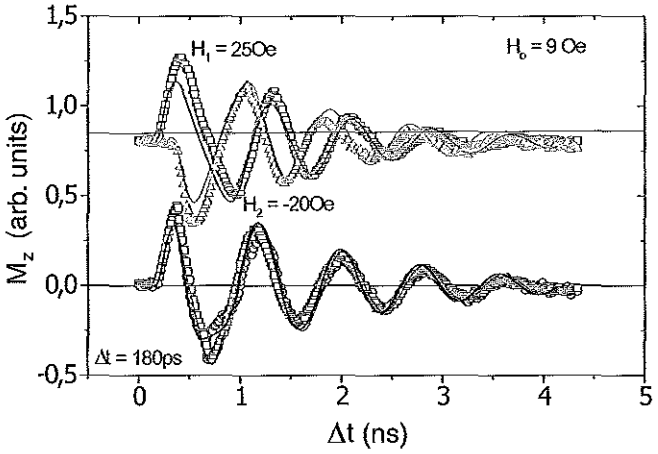

Fig. 11. Dynamics of M_z due to two single magnetic field pulses of opposite sign (*upper part*) and due to their combined effect (*lower part*). *Symbols* are data points; *solid line* in the *lower graph* represents the sum of the individual excitation data shown in the *upper part* [28]

respectively. The quenching pulse was started at the maximum excursion of M out of the thin-film plane. The *open squares* in the lower graphs correspond to the system's response to the combination of the two currents. The graph clearly shows that the motion directly after launching the quenching pulse is accelerated by the sudden increase in the torque acting on M due to the bias and anisotropy field present. The *solid line* represents the superposition of the individual excitation data of the first pulse and the quenching pulse. A clear difference between the superposition of the data and the experimentally observed response due to the shaped pulse can be observed, which originates in the nonlinearity of the magnetic response (the effective field depends on M).

2.2.2 Stopping the Precession without Reversal

Our system with two individual photoswitches now allows us to tune the magnetic field pulse by adjusting the delay and amplitude of the second pulse, in this way stopping the precessional motion, as shown in Fig. 12. The initial excitation was carried out by a 30-Oe field pulse (open circles). The bias field of 49 Oe guarantees that the maximum excursion is smaller than 60° and that no reversal occurs. The quenching pulse follows the first pulse 502 ps later with an amplitude of −20 Oe (open squares). It compensates for, i.e., it quenches, the field due to the first switch at its trailing edge. This compensation is almost perfect due to the exponential character of the decay. The response due to the shaped pulse is represented by the open triangles. Clear stopping of the system's motion can be observed after one

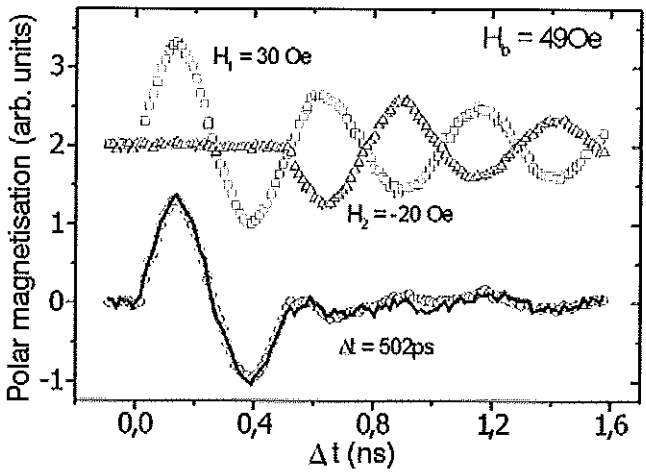

Fig. 12. The precession of M is stopped by using two pump pulses of 30 and -20 Oe, respectively, separated in time by exactly one precession period (here 502 ps). *Top graphs* show the response to individual field pulses; *bottom graph* shows the combined effect leading to almost perfect suppression of ringing [28]. The *solid line* in the bottom graph is the sum of the individual excitation data and completely overlaps the experimental results obtained for the combined effect

full round-trip when M passes the thin-film plane. At this moment, the usually large vertical demagnetizing field is zero, and the in-plane quenching pulse aligns H_{eff} parallel to M. Now, the nonlinearity plays a minor role, and the excursion from equilibrium due to the first signal is negligible. The solid line in Fig. 12 is the superposition of the two independent signals; it shows no difference with regard to the shaped field excitation, indicating that the magnetization state is the same when the total field is quenched.

2.2.3 Large-Angle Excitation with Reversal

For the switching experiments, the patterned magnetic structures are elliptically shaped 8-nm thin Permalloy films, situated on the strip line just in front of the taper. The elliptic shape of the elements was chosen to achieve a uniform demagnetization field that is expected to facilitate uniform switching. Large-angle excitation is achieved by applying a 70-Oe amplitude field pulse and a bias field of only 10 Oe. The bias field is just strong enough to evoke a uniform initial magnetization state; the elliptical shape of the element guarantees uniformity of the demagnetizing field and thus of the torque on the spins, as long as the motion is coherent. For fast switching, coherence of the system is indispensable, implying that the magnitude of the mean magnetization in the spot area does not change. Therefore, we measured all three magnetization components, the in-plane ones by MSHG and the polar component by polar MOKE.

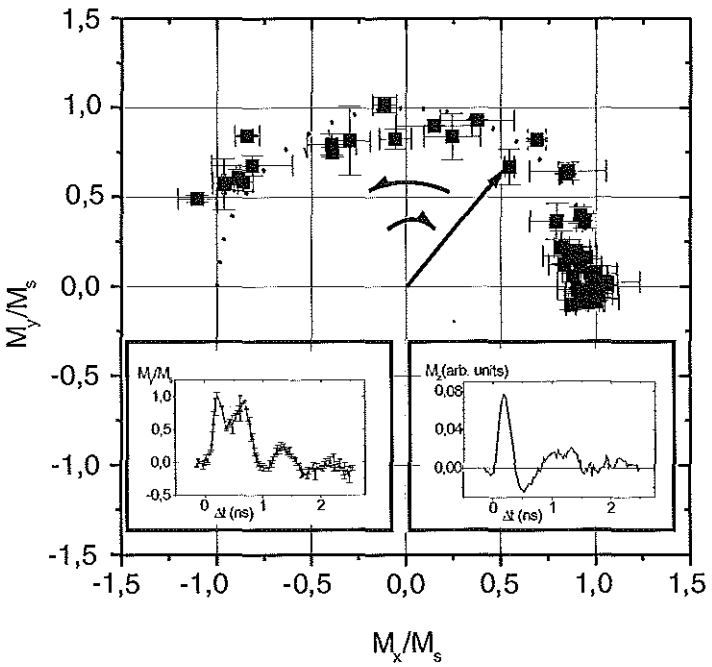

Fig. 13. In-plane (xy) projection of large field excitation without stopping pulse, as probed by MSHG. The ringing effect is still present, as shown in the insets representing the response of the y and z components of M, respectively. After a maximum excursion of 160°, the nonzero torque acting on M drives the magnetization back to its initial state [29]

Figure 13 shows the data obtained for the large pulse excitation. A 160° rotation of M could be observed. The in-plane projection of M clearly shows that the magnetization is coherent inside the spot area. Note that the polar component is negligible, as follows from the nonchanging amplitude of the in-plane magnetization component. The dynamics of the M_y component along the field pulse and the polar M_z component, shown in the insets of Fig. 13, demonstrate that ringing of the magnetization motion after reversal is due to the fields acting. The coherence of the rotation in the elliptical element has been further verified by measuring the x and y components of M for five different spots on the element that showed exactly the same response. The 3 d probing of M allows us to follow the trajectory of M in space and time. This three-dimensional trajectory of M is shown in Fig. 14. (Note that the polar M_z component is given in arbitrary units and has been enlarged for clarity.)

Figures 13 and 14 show that a strong excitation pulse (here, 70 Oe) alone is not sufficient to obtain switching because the combined fields that act on M at its maximum excursion ($\approx$ 160°, i.e., almost reversed) give rise

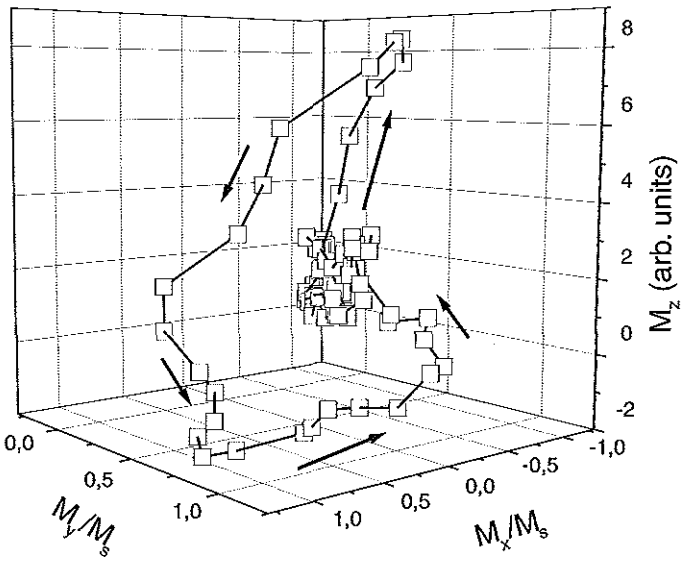

Fig. 14. 3d trajectory of M probed by MSHG (in-plane) and polar MOKE. Note that the polar component is enlarged for clarity [29]

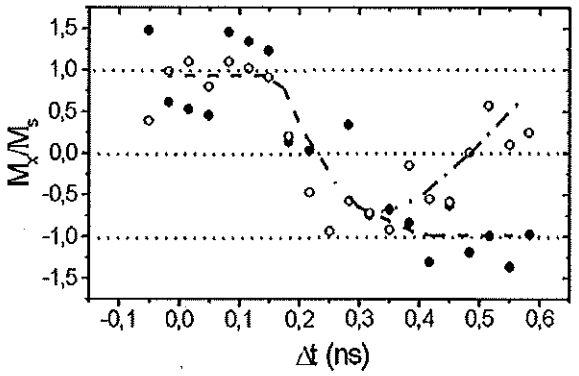

Fig. 15. Strong pulse stop: After maximum excursion of M by a strong field, a quenching field is sent, by which the motion of M is terminated and finally reversed [29]

to a strong torque that drives M back to its starting direction. To obtain actual switching, the delay of the quenching pulse must be adjusted so that the motion is stopped at half the precessional period. Figure 15 shows the response of the magnetic system with and without such a quenching-field pulse. The quenching field is launched at the maximum in-plane excursion from the initial state, so that its cancelation becomes effective when M_z is zero and M is reversed.

A clear magnetization reversal, now followed by stopping of the motion and thus suppression of the ringing is observed when the quenching pulse is present. Note that this reversal is reached in about 200 ps, which is about an order of magnitude faster than the natural damped motion, with a typical time constant of 1.5 ns (see Fig. 6). This indicates a possible switching rate of 5 GHz for the present configuration.

These results show that by proper engineering of magnetic field pulses, very fast switching of magnetic elements is possible. Using multiplexing of many parallel pulses, this would imply tremendous opportunities for applications in MRAM devices (see also Sect. 2.2.4 below). One might argue that femtosecond laser pulses may not be very suitable for large-scale applications in real devices. However, so far, state-of-the-art electronic pulse generators have a hard time generating the required short (100-ps) current pulses (see chapter by *Russek* et al.). In particular, their temporal stability (jitter) is often of the same order as the required pulse width, thereby hindering perfect suppression of ringing. In our technique, on the contrary, the only sources of jitter are variations in the optical path length that are restricted to the femtosecond regime.

2.2.4 Application to MRAMs

Based on the experimental results presented in Sect. 2.2.3, we can now see what the implication of our technique would be for application to a magnetic random access memory (MRAM) device. The progress in magnetic tunnel junction (MTJ) technology has stimulated an enormous effort to develop MRAMs. In such MRAMs, each memory element consists of a MTJ in between a magnetic layer with fixed magnetization and a softer magnetic layer with uniaxial anisotropy by which the two binary states are defined. In a practical situation, one is forced to replace the hard layer by complicated multilayer structures to guarantee the stability of its magnetization [44]. Writing information then corresponds to switching the soft layer relative to a fixed one.

The present study has direct implications for the operation of MRAM cells because the properties of their memory layer (soft layer) correspond to the characteristics of the elements investigated above. Using our experimental results, we can access the consequences of our switching method for these memory devices.

A MRAM consists of a matrix of word and bit lines, as shown in the inset of Fig. 16. A memory element is located at each crossing of a bit and word line. The element, whose magnetic state has to be defined, is selected by the crossing of those bit and word lines, through which current pulses are sent. The aim is to define the direction of M in the element(s) at the crossing and leave the magnetization states of all other elements along these lines unchanged. The technique presented uses pulses of single polarity, by which the binary state of the magnetic element is reversed independently of

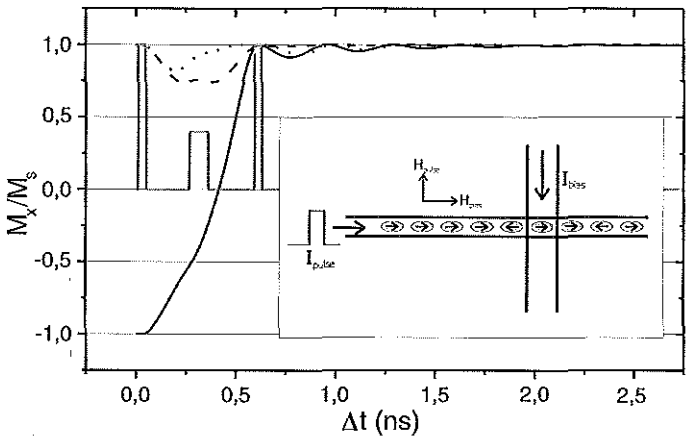

Fig. 16. Simulations based on the experimental switching results show a possible application of the pulse-shaping technique to the future MRAM. Ultrafast switching with single polarity pulses on the bit line and suppression of ringing after excitation is possible. The *inset* shows the scheme of a typical MRAM cell [30]

its initial state when no bias field is present. In the MRAM, the bias field is provided by the word line current. The bias field can be either parallel or opposite to M in the selected element. In both cases, the dynamic changes should occur without ringing.

That this is possible is clearly demonstrated in Fig. 16 which shows simulations on the basis of the Landau–Lifshitz equation. Bear in mind that all reversals shown in the sections above could well be simulated by this equation while using the same set of intrinsic parameters, so that we should expect good reliability from these simulations. Both the reversal (*solid line*) and the return to the initial state (*dotted line*) should take place without oscillations about the equilibrium. The torque on the other elements along the selected word line is about zero because the field and the magnetization are about parallel. However, the motion of the other elements on the selected bit line, which experience an orthogonal field, must also be terminated without oscillation. It can easily be shown by simulations that these elements can unintendedly be switched by subsequent write actions, when they are not stabilized properly. However, by an adequate sequence of pulses, the ringing of these elements can simultaneously and efficiently also be suppressed (see *dashed line*). As clearly demonstrated in Fig. 16, all of these demands can simultaneously be accomplished by a single-polarity bit-line field pulse, consisting of three independent pulses, for a given bias field on the word line. This pulse sequence consists of an excitation pulse, one intermediate pulse, and the stop pulse. The concept of biased excitation with suppression of ringing by a sequence of two pulses has already been demonstrated in [28]. The intermediate pulse is needed to get all possible individual responses in phase,

so that the subsequent stop pulse suppresses ringing for all possible excited states.

At this point, we should briefly discuss alternative approaches toward magnetic field-pulse switching, as were recently demonstrated by both the NIST [31] and Orsay groups [32]. In comparison with our approach, these groups use high-bandwidth electronics instead of ultrafast lasers, allowing the generation of magnetic field pulses with typical rise times of 50–100 ps and minimum pulse duration of 100–200 ps. As shown above (and explained in more detail in the chapter by *Russek* et al.), for coherent rotation, one needs both a high enough pulse amplitude and a short enough pulse rise time and pulse duration. From an experimental point of view, a major advantage of the optical approach is its extreme stability, i.e., the total absence of jitter (limited to a few femtoseconds) in comparison with the typical values of 10–50 ps for high-bandwidth electronics. The price one pays for this is, of course, a slightly more evolved experimental setup.

2.3 Summary

We have developed a technique that allows controlling the precessional motion of a ferromagnetic system on a picosecond timescale. Pronounced precessional ringing after excitation can be suppressed and the precessional motion of the system can be controlled. Large field-pulse excitation showed oscillation after reversal in elliptically shaped elements. A stop pulse can terminate that motion when M is in a local energy minimum at the maximum excursion angle. With this technique, control of ultrafast precessional magnetization reversal in critically underdamped systems with switching rates of at least several GHz is possible. We have also shown, by simulations, that this technique can be used to improve the switching rate and the data integrity in MRAM devices.

3 Laser-induced Switching of Magnetic Media

Magnetic recording started in the early 1940s and the resulting tape recording technique still prevails today, though it is rapidly being replaced by alternatives in the past decade. Apart from audio and video applications, magnetic recording has found large-scale application in backup and archival storage of information.

3.1 Magneto-Optical Recording – Introduction

Since the start of the computer industry in the late 1950s, magnetic hard disks have been used as mass storage devices and achieved an exponential growth of bit density that is now close to 100 Mbits/in^2. Despite strong developments of MRAMS and other alternatives, magneto-optical (MO) recording

is still one of the most important technologies for removable storage media. In particular, new developments like the invention of magnetically amplified magneto-optical systems (MAMMOS) [36] has led to an enormous improvement in accessible bit densities of up to 23 Gbits/in^2 [37]. Because the corresponding size of recorded bits is far too small to give a reasonable magneto-optical effect, their magnetic state is first copied to a so-called read-out layer and subsequently amplified within this layer by domain expansion due either to an external magnetic field or the intrinsic magnetic properties of the read-out layer itself (zero-field MAMMOS). Both processes, copying and expansion, are governed by transient temperature profiles that are induced by the focused laser beam that is also used for reading the information and are thus closely related to conventional thermomagnetic writing. The quality of magneto-optical disks depends on high bit densities and perfect read reliability and also on bit writing speed and access time, so the dynamics of thermomagnetic writing drew high technological interest again.

In this section, time-resolved polar Kerr effect data on femtosecond pump-pulse-induced magnetization reversal of a typical MO read-out layer is presented for various pump fluences. Three different configurations of an external field H_{ext} were chosen to study (i) temperature-induced magnetization dynamics within single domain states, (ii) pump-pulse-induced magnetization reversal, and (iii) the dynamics of remanent magnetization.

Temperature-induced magnetization dynamics showed ultrafast magnetization collapse within 1ps followed by slower recovery whose speed was limited by the cooling rate. Reversal dynamics was governed by a convolution of temperature-induced changes in the magnitude of M and of transient rotation of its direction driven by the external field. Rotational dynamics followed the Bloch equation via a reversal time that does not depend on temperature but strongly decreased with increasing pump fluence. For the highest applied pump fluence, leading to temperatures far above the Curie point, a reversal time of less than 2 ps was found, whereas about 1 ns was required for the sample to cool down to room temperature again. This result indicates that writing rates of several 100 GHz can be achieved for samples with accordingly fast cooling rates. A comparison of data obtained in an external saturation field and in remanence opened the way to separating the contributions due to temperature-induced effects within single domains from those related to field-induced domain formation.

3.2 Thermomagnetic Writing – Basics

Thermomagnetic writing is the process in which a focused laser beam together with an applied magnetic field creates a reversed magnetic domain in a magnetic thin film (see Fig. 17). The concept is simple and can be sketched as a three-step process: (i) the focused laser beam creates a hot spot where the coercive field decreases below the oppositely directed external field, (ii) barrier-less magnetization reversal takes place in this hot spot and

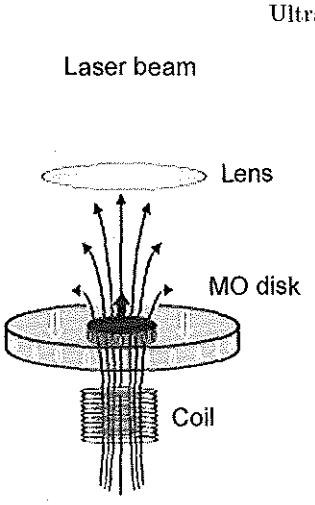

Fig. 17. The principle of thermomagnetic writing: the external field (here generated by a coil) can reverse only the central spot heated by the focused laser beam

aligns the magnetization along the external field, and (iii) the sample cools down again. Accordingly, the dynamics of thermomagnetic writing is limited by the duration of these three processes.

In practice, thermomagnetic writing is a complex process involving the nucleation of an initial reversed domain, followed by its expansion and stabilization while the heating and cooling of the usually rotating medium takes place. The dynamics of the nucleation and growth of domains for quasi-static writing have been studied extensively in the past decades (see, for example, [39,40,41]), but a quantitative description is still hard to achieve. It is clear that the microstructure of the MO media plays an important role because thermomagnetically recorded domains in a truly uniform and homogeneous medium are not stable. The same will be true for the writing process using pulsed lasers, with the additional point that the enormous temperature gradients that can be achieved by pulsed-laser excitations, may directly influence the microstructure itself.

The magnetic medium typically must have a combination of particular properties. Large perpendicular anisotropy, resulting in out-of-plane magnetization, is required for reading the magnetic information by using the polar Kerr effect; a large coercive field that decreases strongly with temperature is necessary to obtain sufficient stability of the recorded bits at room temperature and to reverse the magnetization at elevated temperatures by means of moderate fields; good thermal conductivity is required for fast cooling, etc. These material characteristics must furthermore match the recording conditions, i.e., laser power, rotational speed, applied field, etc. A comprehensive overview of thermomagnetic writing can be found in the *Physical Principles of Magneto Optical Recording* by *Mansuripur* [38]. Most materials used for MO recording are amorphous alloys of rare-earth (RE) and transition metal (TM) elements and are ferrimagnetic, that is, the magnetization of the RE and TM sublattices are antiferromagnetically coupled; see Fig. 18. This coupling be-

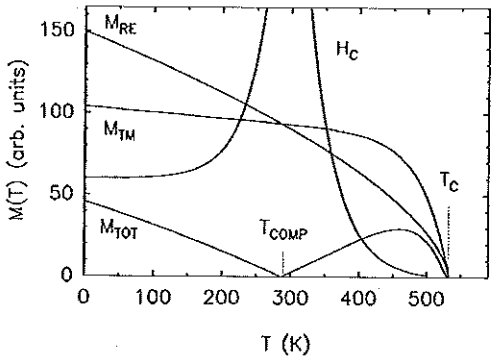

Fig. 18. Typical temperature dependences of the magnitudes of rare-earth (RE) and transition-metal (TM) subsystem magnetization, total magnetization (TOT), and of the coercive field H_C for MO materials. Antiferromagnetic coupling between RE and TM magnetization leads to a compensation temperature T_{comp} where $M_{TOT} = 0$ and also to a common Curie temperature T_C

tween the two sublattices is responsible for the fact that there is only one T_C. Because the magnetization of an RE sublattice (M_{RE}) is larger than that of a TM sublattice (M_{TM}) at low temperatures but decreases faster when the sample is heated, a so-called compensation temperature exists, where both magnetizations are equal. At this temperature, the net magnetization is zero, and the coercive field diverges as shown in Fig. 18. These characteristics can be well described by a coupled mean-field theory [42] and are very important for the process of magnetic amplification.

3.3 Ultrafast Dynamics of Thermomagnetic Writing

In this section, we want to investigate the dynamics of thermomagnetic writing, using ultrashort (fs) laser pulses to heat the MO media. In general, these dynamics can again be discussed within the previously mentioned three steps of heating, reversal, and cooling, but now different mechanisms can be responsible for the dynamics within each step. Regarding femtosecond laser-pulse-induced temperature dynamics, it is well known that optical excitation of electrons first leads to a fast temperature rise within the electron system, whereas the lattice remains almost at ambient temperature at this time [43]. The subsequent electron temperature relaxation is governed by electron–phonon collisions and heat diffusion within the electron gas. Whereas electron–phonon collisions are responsible for equilibration of the electron and phonon systems by heating up the lattice, heat diffusion will enlarge the depth of the heated region. Consequently, the initial breakdown of magnetization and the coercive field can be induced by heating the lattice and also by the fast transient of the electron temperature as well. In addition to temperature effects, spin flips of single optically excited electrons (Stoner excitations) may also

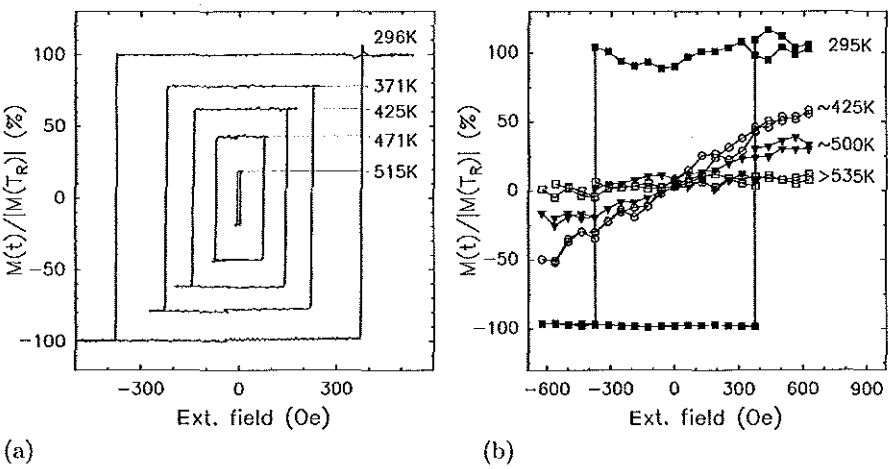

Fig. 19. Hysteresis loops measured on our sample for distinct equilibrium (a) and transient (b) temperatures. Transient temperatures were fixed by measuring at distinct pump-probe delays (295 K: negative delay; $>$ 532 K: $\leq$ 67 ps; $\sim$ 500 K: 267 ps; $\sim$ 425 K: 667 ps)

influence initial dynamics [45]. Although the action of the external field on magnetization is expected to be identical for conventional and femtosecond laser-pulse-induced thermomagnetic writing, the microscopic structure of M that is created during the initial heating stage might differ significantly in both cases. Such differences will then affect the subsequent reversal dynamics. That slow heating and fast optical excitations lead to different magnetic states is indicated in Fig. 19, where hysteresis loops measured for similar values of the equilibrium and the transient lattice temperature are compared.

Now the question arises, how do we analyze the measured dynamics of femtosecond laser-pulse-induced magnetization reversal? With regard to the first heating step, we expect that temperature-induced magnetization dynamics for delay times longer than 2 ps will be governed by the transient electron temperature via the equilibrium magnetization curve [4,6,7]. But what about reversal dynamics? At constant temperature, barrier-less magnetization reversal induced by an external field $\boldsymbol{H}_{\mathrm{ext}}$ that is oriented antiparallel to the initial magnetization direction (z direction) obeys the Bloch equation,

$$\frac{\mathrm{d}M_z(t)}{\mathrm{d}t} = -\frac{M_{0,z} - M_z(t)}{\tau}\,, \tag{4}$$

where $M_{0,z}$ denotes the final equilibrium position of the reversed M_z pointing in the direction of the external field and τ represents the material-specific reversal time[1]. The meaning and behavior of τ depends on the microscopic

[1] Note that the Landau–Lifshitz–Gilbert equation (introduced in Sect. 1.1, to describe the magnetic response to field pulses) predicts no response of the macro-

reversal mechanism. For incoherent rotation of M within a single domain state, τ is given by the electron spin–lattice relaxation time which depends on temperature but not on the effective field H_{eff} [46]. When reversal is due to nucleation and the growth of oppositely directed domains, on the contrary, τ will be insensitive to temperature but depends on H_{eff} [47]. Thus, measurements of the temperature and field dependence of τ may uncover the microscopic reversal mechanism. Using the relation $M_z(t) = |M| \cos \Phi(t)$, it is obvious that the Bloch equation is intrinsically an equation of motion for $\cos \Phi$:

$$\frac{\mathrm{d} \cos \Phi(t)}{\mathrm{d}t} = -\frac{\cos \Phi(t) + 1}{\tau}, \tag{5}$$

with the well-known solution

$$\cos \Phi(t) = \cos \Phi(t = 0)(2\mathrm{e}^{-t/\tau} - 1). \tag{6}$$

The latter formulation of the Bloch equation does not depend on the actual magnitude of magnetization and can consequently be used to describe the dynamics of thermomagnetic writing and hence, of femtosecond laser-pulse-induced magnetization reversal as well. Prerequisite for the validity of this approach is that the transient temperature and transient magnetization have to be in thermal equilibrium at any time, i.e., the actual magnitude of magnetization has to be related to the actual temperature via the equilibrium magnetization curve. This has to be checked by additional measurements of purely temperature-induced magnetization dynamics, so we will present and discuss data that are obtained for the following three different configurations of the external field H_{ext}:

(i) H_{ext} is a saturation field that suppresses any domain formation – only temperature-induced magnetization dynamics is measured.
(ii) H_{ext} is antiparallel to M and smaller than H_{C}^0, the coercive field at ambient temperature – magnetization dynamics will be governed by temperature-induced changes in $|M|$ and field-driven reversal of $\cos \Phi$.
(iii) $H_{\text{ext}} = 0$ – data will clarify whether magnetization dynamics in remanence is governed solely by temperature effects or also influenced by the dynamics of the effective field in the sample. Before presenting the results, we will introduce the experimental background of our measurements.

3.4 Experimental Procedure

3.4.1 Sample

The sample was a typical MO multilayer structure grown by magnetron sputtering on a glass substrate. An uppermost 50-nm thick film of SiN protected

scopic magnetization vector M for antiparallel orientation of M and H_{ext}. However, it is widely used as the basis for micromagnetic calculations on thermomagnetic writing [38]

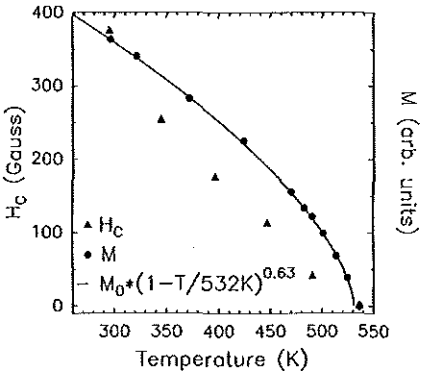

Fig. 20. Temperature dependence of the coercive field and TM magnetization of the sample investigated

an underlying 30-nm thick film of α-$Gd_{23.1}Fe_{71.9}Co_{5.0}$ from degradation. The α-$Gd_{23.1}Fe_{71.9}Co_{5.0}$ was in turn grown on 5 nm SiN to get identical interfaces for the ferrimagnetic film. The structure was completed by an AlTi film 100 nm thick, which served as heat sink and enhanced the reflectivity of the whole structure. The sample showed strong out-of-plane anisotropy and its Curie and compensation temperatures were 532 K and 260 K, respectively. Variations in the coercive field and the TM magnetization with temperature derived from linear measurements of the polar Kerr effect are shown in Fig. 20.

3.4.2 Optical Setup

A schematic representation of our optical setup is shown in Fig. 21. Laser pulses of 100 fs duration and 800 nm wavelength, generated by a commercial amplified laser system at a repetition rate of 20 Hz, were sent through a variable attenuation unit before entering a conventional pump-probe setup. The pump beam was at normal incidence and focused to about 1 mm (FWHM), whereas the probe beam was incident on the sample at 30° and focused much more tightly to 100 μm. The probe pulses contained about 4×10^3 times less energy than the pump pulses to get negligible self-action. A balanced diode scheme was used to detect only the polar Kerr rotation. Measuring the polar Kerr rotation with 800-nm wavelength light, we were solely sensitive to the TM magnetization [48].

3.4.3 External Field

The external field was applied along the easy axis perpendicularly to the sample surface by mounting the sample on top of the soft iron core of the electromagnet used. The magnetic field was of square-wave form and phase-locked to the laser repetition rate of 20 Hz (see Fig. 22). Its strength at the times between two subsequent pump-probe pulse pairs, H_{off}, was larger

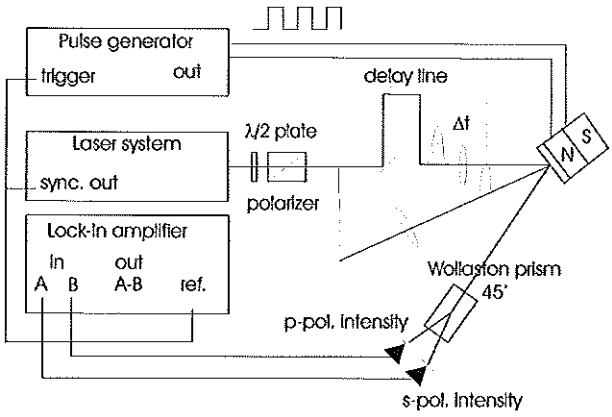

Fig. 21. Scheme of the experimental setup for monitoring the femtosecond laser-pulse-induced reversal dynamics

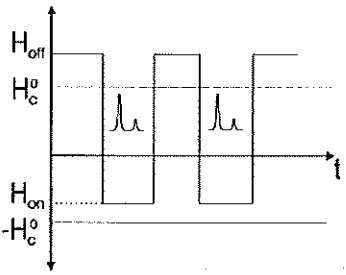

Fig. 22. Scheme of the external magnetic field applied synchronously with pump-probe laser pulses

than the coercive force of the sample at room temperature, H_C^0, to guarantee identical initial conditions for each pulse pair. In this way, the magnetization of the sample was always saturated before each pump-pulse excitation. Thus, the signal-to-noise ratio could be improved by averaging the signals of several probe pulses without losing access to the real magnetization dynamics [3,12]. Figure 23 shows the relevance of this approach. Without using the square-wave magnetic field, the hysteresis loop for negative time delay (i.e., before the pump pulse) changes dramatically.

The direction and magnitude of the external field affecting the sample at the times when pump and probe pulses were reflected at the sample, H_{on}, were chosen in accordance with the three previously mentioned configurations as (i) $H_{on} = H_{off}$, (ii) $H_{on} = -2/3H_C^0$ (oppositely directed to H_{off}), and (iii) $H_{on} = 0$.

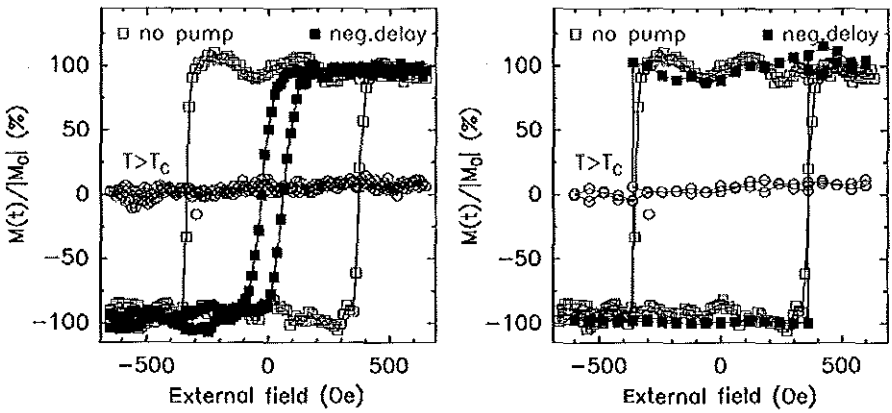

Fig. 23. Comparison of typical hysteresis loops measured by application of a quasi-static field (*left*) and by application of a square-wave field (*right*). For quasi-static fields, an apparent reduction of the coercive field is observed that reflects changing initial conditions during the averaging measurement

3.5 Femtosecond Laser-induced Dynamics

In this section, we will discuss how the use of the three field configurations allows us to separate the various (field and temperature) induced contributions to magnetization dynamics.

3.5.1 Temperature-induced Dynamics

To measure changes in M that were caused exclusively by transient electron and lattice temperatures, we applied a constant saturation field $H_{\mathrm{on,sat}}$. Corresponding results obtained for a pump fluence of $\approx 5.4\,\mathrm{mJ/cm^2}$ are shown in Fig. 24. In the upper panel (a), the initial magnetization dynamics, identical for both magnetization directions, is compared to simultaneously measured changes of linear reflectivity which monitor the temporal evolution of the electron temperature T_e. Very fast and complete breakdown of magnetization during the first picosecond is observed, which is about 500 fs delayed with respect to the increase in T_e. Measured and calculated dynamics of the subsequent magnetization recovery at longer delay times are compared in the lower panel, Fig. 24b. The calculation was based on the assumption that $|M(t)| = |M[T(t)]|$ is governed by the electron temperature via the equilibrium magnetization curve (see Fig. 20). Excellent agreement between data and calculation is found which proves that the recovery of magnetization is solely determined by cooling of electrons. This result is in line with the behavior of itinerant ferromagnets reported in the literature [3,4,5,6,7] and justifies using (5) to analyze transient magnetization reversal.

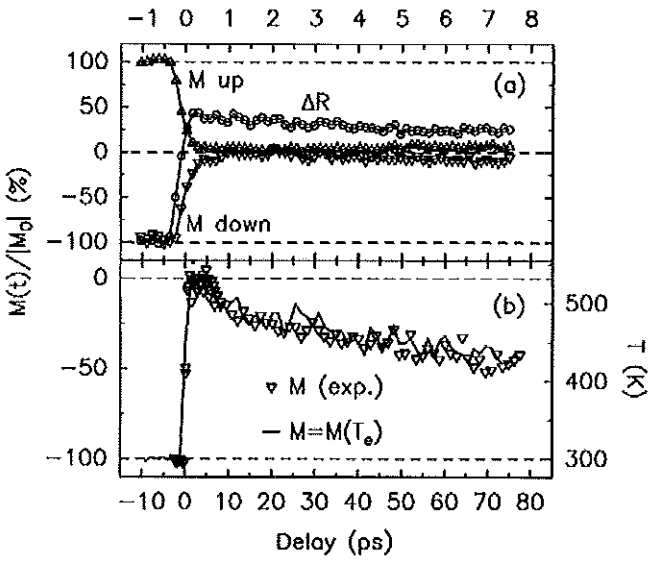

Fig. 24. Magnetization of the TM subsystem of GdFeCo normalized to its magnitude at room temperature as a function of pump-probe delay. (a) Comparison of the initial magnetization dynamics to simultaneously measured changes in linear reflectivity (ΔR) by monitoring the transient electron temperature T_e. (b) The measured recovery of M at longer delays (*symbols*) compared with the theoretical expectation (*solid line*) which is obtained by transforming the measured $\Delta R(t)$ into transient magnetization via the equilibrium magnetization curve

3.5.2 Ultrafast Magnetization Reversal

The dynamics of femtosecond laser-pulse-induced magnetization reversal is governed by both temperature-induced changes in $|M|$ and field-induced rotational dynamics, $\cos\Phi(t)$. To gain insight into these two contributions experimentally, we proceed as follows: First we measure, for one fixed pump fluence, both the dynamics that is solely induced by the transient temperature (sample exposed to a constant external saturation field $H_{\mathrm{on,sat}}$) and the reversal dynamics driven by an external field $H_{\mathrm{on,opp}} = -2/3H_{\mathrm{C}}^{0}$. Then, we multiply the measured temperature-induced dynamics by the expected exponential time dependence of $\cos\Phi(t)$ (6) and fit the result obtained to the measured reversal dynamics by varying τ. To minimize possible systematic measurement errors due to slow fluctuations of laser power, we periodically switched the external field from $H_{\mathrm{on,opp}}$ (reversal) to $H_{\mathrm{on,sat}}$ (temperature effects) while scanning the pump-probe delay. Corresponding data and fit results obtained for two different pump fluences are shown in Fig. 25.

For low pump fluences, such as $F_{\mathrm{pump}} = 4.0\,\mathrm{mJ/cm^2}$, as used in the experiment shown in Fig. 25a, very fast magnetization breakdown is followed by a recovery of M_z for both temperature-induced dynamics $M_z(t) = |M(t)|$ (*big open up-triangles*) and even the reversal dynamics $M_z(t) = |M(t)|\cos\Phi(t)$

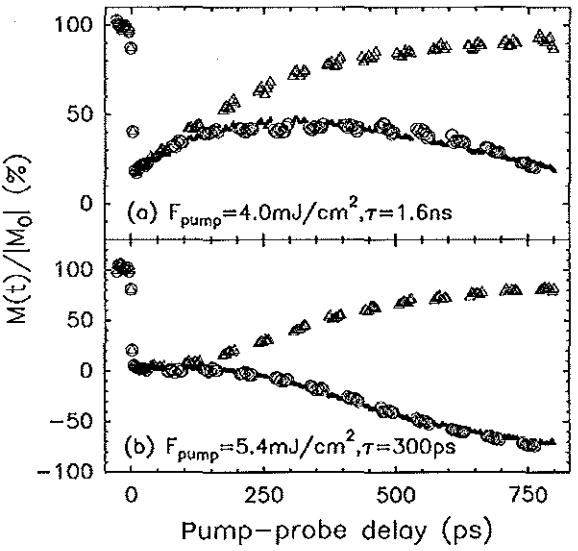

Fig. 25a,b. Measured time-dependences of both purely temperature-induced dynamics (*open triangles*) and reversal dynamics (*open circles*) for two pump fluences. The small *solid symbols* in between the data of the reversal dynamics represent the measured temperature-induced dynamics multiplied by the theoretically expected rotational dynamics (6) using temperature-independent reversal times τ of 1.6 ns and 300 ps, respectively

(*big open circles*). Such behavior is expected when the recovery of $|M|$ due to cooling is faster than the field-driven rotation $\cos\Phi$. That the dynamics of $\cos\Phi(t)$, in this case, is very slow was proven by the result of the previously outlined fit procedure (*small solid up-triangles*) yielding a temperature-independent reversal time of $\tau = 1.6 \pm 0.3$ ns.

High pump fluences, in contrast, lead to much shorter reversal times and the reversal dynamics shows no recovery of M_z (Fig. 25b). The results of additional measurements of the reversal dynamics with other pump fluences but the same external field of $H_{\mathrm{on,opp}} = -2/3H_{\mathrm{C}}^{0}$ are shown together with corresponding fits in Fig. 26. Each individual data set is excellently fitted by (5). This finding proves that the temperature-induced breakdown and recovery of TM magnetization and also its reversal dynamics are in line with the behavior of pure ferromagnets because (5) does not account for the coupling between the TM and RE moments. Despite the fact that the temperature varied over a large range up to 200 K for the highest pump fluences, all fits yielded one constant value of $\tau \pm 20\%$ for each data set. This demonstrates that τ does not depend on temperature and points to transient domain formation as the microscopic reversal mechanism.

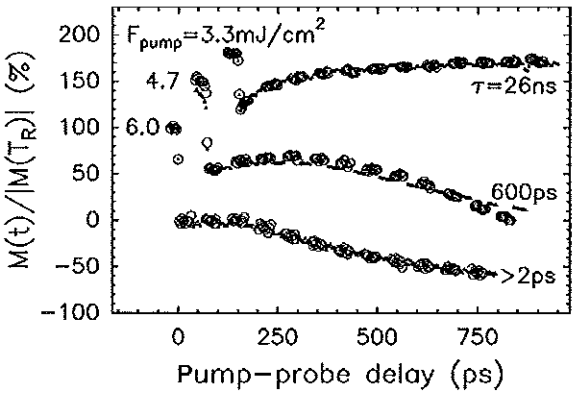

Fig. 26. Transient magnetization reversal dynamics (*symbols*) measured for distinct pump fluences, F_{pump}. *Solid lines* represent best fits of (5) to the data multiplied by the temperature-dependent magnitude of M. Values of F_{pump} (in units of mJ/ cm^2) and of the fitted reversal times are given. The data are offset for clarity

3.5.3 Reversal Mechanism

As pointed out above, the observation that the reversal time τ in our experiment does not depend on temperature suggests transient domain formation as the mechanism for reversal. However, the reversal due to transient domain formation depends on the strength of the coercive field, and constant values of τ are expected only when the variations in H_C are restricted to the first few picoseconds. We checked this prerequisite by measuring hysteresis loops at distinct pump-probe delays. The results of these measurements, already presented in Fig. 19, demonstrate that H_C vanishes within the first 2 ps and remains zero for pump-probe delays up to 667 ps. The observed transition of the shape of the hysteresis loops from rectangular at negative pump-probe delays (reversal within single domain) to continuous changes in M with H at positive delays indicates again that transient domain formation is the microscopic reversal mechanism.

Another striking observation in Fig. 26 is the strong decrease of the fitted reversal times with increasing pump fluence. As shown in Fig. 27, we found that the reversal times obey $\tau = \tau_0 \cdot \exp[9.52|M_{\text{min}}|/|M(T_{\text{room}})|]$ with $\tau_0 = 300$ ps, as long as at least some part of the probed area is not completely demagnetized. Although we have no direct experimental proof of its origin, we suggest that it is related to an increase in the number of initially created nucleation sites and to a simultaneous decrease of exchange coupling to the surroundings. The importance of the surroundings is indicated by the data we obtained for the two highest pump fluences. A value of $\tau = (300 \pm 60)$ ps was found for $F_{\text{pump}} = 5.4\,\text{mJ/cm}^2$, where the Curie temperature was just reached within the probed area (note that this corresponds exactly to the τ_0 defined above). However, no delay between the recovery and reversal dynam-

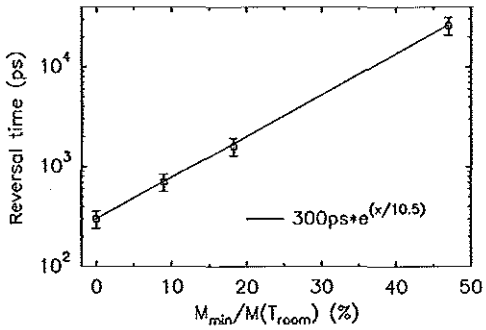

Fig. 27. Reversal times determined (*symbols*) versus $M_{\min}/M(T_{\text{room}})$ (%), where $M_{\min}$ denotes the minimum value of the magnetization that was observed in the corresponding experiment. Smaller values of $M_{\min}$ relate to higher pump fluences. *Solid line* represents the empirical relation given in the figure

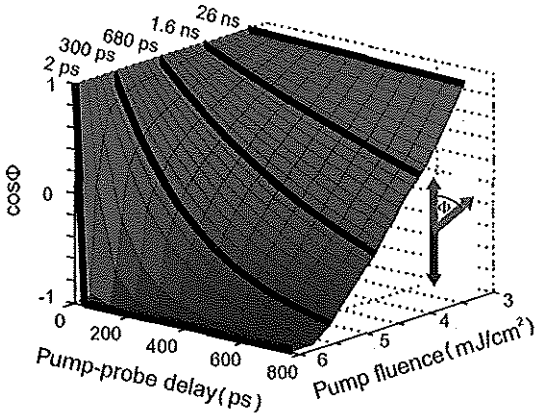

Fig. 28. Time dependence of $\cos\Phi$, i.e., true reversal dynamics, as a function of pump-probe delay and pump fluence. Thick lines represent best fits to all experimental data from Figs. 25 and 26

ics was found for a higher fluence of 6.0 mJ/ cm^2, where the surrounding of the probed spot is also heated above T_C. It would be interesting to perform additional time-resolved microscopy measurements to check these suggestions.

Up to this point, all data and corresponding fits presented reflect the magnetization dynamics that is governed by a convolution of temperature effects (via $|M|$) and rotational dynamics (via $\cos\Phi$). However, our analysis allows us to deconvolute both contributions; the separated dynamics of $\cos\Phi$ is plotted in Fig. 28. The fact that $\cos\Phi$ can be reversed within less than 2 ps demonstrates that the ultimate speed of femtosecond laser-pulse-induced thermomagnetic writing is limited only by the slow cooling rate of the sample.

3.5.4 Magnetization Dynamics in Remanence

Measurements of ultrafast magnetization dynamics in remanence can help to answer the question whether optical excitations by femtosecond laser pulses will lead only to reversible temperature-induced changes in magnetization or may also cause irreversible domain formation. A typical result of a corresponding measurement is shown in Fig. 29 and compared to purely temperature-induced as well as to reversal dynamics that are measured for the same pump fluence.

Obviously, the data measured in remanence strongly deviate from purely temperature-induced dynamics. The perfect agreement with the sum of temperature-induced and reversal dynamics, represented by the *solid line*, indicates the occurrence of irreversible domain formation. This result demonstrates that time- and spin-resolved photoemission measurements in remanence are not sufficient to uncover the nature of femtosecond laser-pulse-induced magnetization dynamics. This might explain the differences in observed magnetization dynamics in nickel investigated by optical techniques in external saturation fields [2,4,7] and by spin-resolved photoemission [45] measured in remanence.

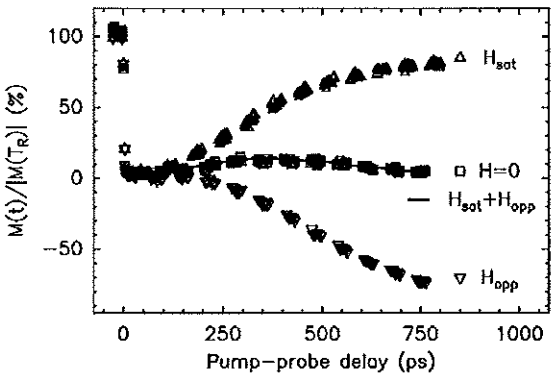

Fig. 29. Comparison of magnetization dynamics measured in remanence (*squares*) to purely temperature-induced dynamics measured in a constant saturation field (H_{sat}, *up-triangles*) and to pump-pulse-induced reversal (H_{opp}, *down-triangles*) measured for an identical pump fluence of $5.4\,\mathrm{mJ/cm^2}$. The *solid line* represents the sum of temperature-induced and reversal dynamics

3.6 Summary

We have shown that thermomagnetic writing using femtosecond lasers can lead to extremely fast magnetization reversal. We have developed an approach that allows us to separate temperature- and magnetic-field-induced dynamics,

in this way demonstrating that the ultimate speed of thermomagnetic writing is limited only by the cooling rate of the medium. Comparing these results with results obtained with the sample in remanence shows that one has to be very careful in interpreting experiments like spin-resolved photoemission, possibly because irreversible domain formation may occur.

4 Conclusion and Outlook

The development of femtosecond laser systems has opened a new area in magnetization dynamics. They enable us to excite magnetic media with ultrashort stimuli like femtosecond laser pulses and picosecond magnetic field or electric current pulses. These new possibilities have already led to exciting observations of magnetization changes on a (sub)picosecond timescale. However, so far these techniques have hardly been exploited for real magnetization switching. In this chapter, we have presented an overview of our latest developments in novel switching methods, namely, precessional switching and ultrafast thermomagnetic writing, which are both based on fast laser excitation.

Regarding precessional switching, we have shown how, by using specifically shaped magnetic field pulses, precessional switching of magnetic elements at its maximum speed, i.e., at half the precessional period, is possible. Switching rates of 5 GHz were thus obtained, indicating tremendous possibilities for MRAM devices.

Unfortunately, the shapes of the elements in actual MRAM devices deviate from ellipticity, which will impact the coherence of the reversal. Therefore, investigations into incoherent processes which involve exploration of wall and spin-wave dynamics are highly desirable. These phenomena will have repercussions on damping of the coherent mode and saturation magnetization. All of these aspects are accessible by the technique presented.

The capability of making short magnetic field pulse is one of the key advantages of our technique which allows the study of spin dynamics with very high time resolution. The rise time of our pulses can be further improved by applying other, more powerful, lithographic techniques and by adapting the designs of the waveguide and switches to these improved technical potentials. In addition, the control of the shape of the magnetic field pulse can be further improved by using additional switches. In that case, our theoretical simulations of the MRAM behavior can also be experimentally confirmed and will give us even more insight into this fascinating area of ultrafast magnetization dynamics.

In thermomagnetic writing, we have shown how to separate temperature-induced changes in the magnitude of magnetization from field-induced reversal dynamics in the direction of M. This separation allowed us to determine characteristic magnetization reversal times that appeared to decrease strongly with increasing pump fluence. For the highest pump fluence that caused a temperature rise far above the Curie point, we found a reversal

time of less than 2 ps, which is even faster reversal than obtained by precessional switching. However, despite this fast reversal time, the cooling rate also limits the maximum speed of thermomagnetic writing, and maximum writing rates of only 1 GHz could be achieved. From this, it follows that future investigations on samples with improved cooling rates are of high interest.

With regard to both techniques presented, it would be of interest to extend the present experimental studies to spatially resolved ones by applying time-resolved microscopic measurements. Our optical setups are optimally suited for spatially resolving magnetization dynamics within the optical diffraction limit, i.e., the nonuniformity in the response could be resolved on a submicron length scale. Future time-resolved microscopic investigations on ultrafast magnetization reversal will provide unique information about the nature of the reversal mechanism for femtosecond laser-pulse-induced switching and also allow us to study the previously mentioned incoherent processes in MRAM devices. The analysis of such experiments will require more sophisticated theoretical models and micromagnetics; providing spatially resolved dynamics for both cases would be an ideal tool. However, the Landau–Lifshitz equation constitutes the basis for corresponding simulation codes, so that it should be further elaborated to adequately incorporate the aspects of thermal fluctuations and spin-wave dynamics into these calculations.

Acknowledgments

The authors would like to thank all the other members of the group and their outside collaborators for their input and help, in particular O. Gielkens, K. J. Veenstra, A. van Etteger, and M. Bilderbeek from Nijmegen; L. Bär from Siemens, Erlangen, Germany; and H. Awano and N. Otha from Hitachi-Maxell, Japan. Part of this work was supported by the Stichting Fundamenteel Onderzoek der Materie (FOM) and by Philips Research Laboratory, Eindhoven.

References

1. M. H. Kryder, F. B. Humphrey: A nanosecond Kerr magneto-optic camera, J. Appl. Phys. **38**, 829 (1969)
2. E. Beaurepaire, J.-C. Merle, A. Daunois, J.-Y. Bigot: Ultrafast spin dynamics in ferromagnetic nickel, Phys. Rev. Lett. **76**, 4250 (1996)
3. E. Beaurepaire, M. Maret, V. Halte, J.-C. Merle, A. Daunois, J.-Y. Bigot: Spin dynamics in $CoPt_3$ alloy films: A magnetic phase transition in the femtosecond timescale, Phys. Rev. B **58**, 12134 (1998)
4. J. Hohlfeld, E. Matthias, R. Knorren, K.-H. Bennemann: Nonequilibrium magnetization dynamics of nickel, Phys. Rev. Lett. **78**, 4861 (1997)
5. J. Güdde, U. Conrad, V. Jähnke, J. Hohlfeld, E. Matthias: Magnetization dynamics of Ni and Co films on Cu(001) and of bulk nickel surfaces, Phys. Rev. B **59**, R6608 (1999)

6. J. Hohlfeld, J. Güdde, U. Conrad, O. Dühr, G. Korn, E. Matthias: Ultrafast magnetization dynamics of nickel, Appl. Phys. B **68**, 505 (1999)
7. B. Koopmans, M. van Kampen, J. T. Kohlhepp, W. J. M. de Jonge: Ultrafast magneto-optics in nickel: Magnetism or optics?, Phys. Rev. Lett. **85**, 844 (2000)
8. G. Ju, A. V. Nurmikko, R. F. C. Farrow, F. F. Marks, M. J. Carey, B. A. Gurney: Ultrafast time resolved photoinduced magnetization rotation in a ferromagnetic/antiferromagnetic exchange coupled system, Phys.Rev. Lett. **82**, 3705 (1999)
9. H. C. Siegmann, E. L. Garwin, C. Y. Prescott, J. Heidmann, D. Mauri, D. Weller, R. Allenspach, W. Weber: Magnetism with picosecond field pulses, J. Magn. Magn. Mater. **151**, L8–L12 (1995)
10. Y. Acremann, M. Buess, C. H. Back, M. Dumm, G. Bayreuther, D. Pescia: Ultrafast generation of magnetic fields in a Schottky diode, Nature **414**, 51–54 (2001)
11. F. Meier, A. Vaterlaus, M. Aeschlimann, M. Lutz, D. Guarisco, F. Milani, H. C. Siegmann: Time-resolved photoemission spectroscopy on ferromagnetic surfaces and thin-films, J. Magn. Magn. Mater. **93**, 523 (1991)
12. J. Hohlfeld, Th. Gerrits, M. Bilderbeek, H. Awano, N. Ohta: Fast magnetization reversal of GdFeCo induced by femtosecond laser pulses, Phys. Rev. B **65**, 012413-1 (2001)
13. T. J. Silva, T. M. Crawford: Methods for determination of response times of magnetic head materials, IEEE Trans. Magn. **35**, 671 (1999)
14. B. Hillebrands, K. Ounadjela (Eds.): *Spin Dynamics in Confined Magnetic Structures I* (Springer, Berlin, Heidelberg 2002)
15. M. R. Freeman, R. R. Ruf, R. J. Gambina: Picosecond pulsed magnetic fields for studies of ultrafast magnetic phenomena, IEEE Trans. Magn. **27**, 4840 (1991)
16. M. R. Freeman, M. J. Brady, J. Smyth: Extremely high frequency pulse magnetic resonance by picosecond magneto-optic sampling, Appl. Phys. Lett. **60**, 2555 (1992)
17. D. H. Auston: Impulse response of photoconductors in transmission lines, IEEE J. Quantum Electron. **19**, 639 (1983)
18. U. D. Keil, D. R. Dykaar, A. F. Levi, R. F. Kopf, L. N. Pfeiffer, S. B. Darak, K. W. West: High-speed coplanar transmission-lines, IEEE J. Quantum Electron. **28**, 2333 (1992)
19. U. D. Keil, D. R. Dykaar: Ultrafast pulse generation in photoconductive switches, IEEE J. Quantum Electron. **32**, 1664 (1996)
20. M. Y. Frankel, S. Gupta, J. A. Valdmanis, G. A. Mourou: Attenuation and dispersion characteristics of coplanar transmission lines, IEEE Trans. Microwave Theory Technol. **39**, 910 (1991)
21. U. D. Keil, H. J. Gerritsen, J. E. M. Haverkort, H. J. Wolter: Generation of ultrashort electrical pulses with variable pulse widths, Appl. Phys. Lett. **66**, 1629 (1994)
22. O. Gielkens, L. M. F. Kaufmann, E. Smalbrugge, M. R. Melloch, R. H. M. Groeneveld, Th. Rasing, H. van Kempen: Ultrafast phenomena XI, Proc. 11th Int. Conf. (1998) p. 162
23. T. M. Crawford, C. T. Rogers, T. J. Silva, Y. K. Kim: Transverse and longitudinal second-harmonic megneto-optic Kerr effect observed from Ni_8Fe_{19} thin-film structures, IEEE Trans. Magn. **32**, 4087 (1996)

24. W. Bailey, P. Kabos, F. Mancoff, S. Russek: Control of magnetization dynamics in $Ni_{81}Fe_{19}$ thin films through the use of rare-earth dopants, IEEE Trans. Magn. **37**, 1749 (2001)
25. M. Bauer, R. Lopusnik, J. Fassbender, B. Hillebrands: Suppression of magnetic-field pulse-induced magnetization precession by pulse tailoring, Appl. Phys. Lett. **76**, 2758 (2000)
26. T. M. Crawford, P. Kabos, T. J. Silva: Coherent control of precessional dynamics in thin film Permalloy, Appl. Phys. Lett. **76**, 2113 (2000)
27. Th. Gerrits, H. A. M. van den Berg, J. Hohlfeld, O. Gielkens, K. J. Veenstra, K. Bal, Th. Rasing: Precession dynamics in NiFe thin films, induced by short-magnetic in-plane field pulses generated by a photoconductive switch, J. Magn. Soc. Jpn. **25**, 192 (2001)
28. Th. Gerrits, H. A. M. van den Berg, J. Hohlfeld, O. Gielkens, L. Bär, Th. Rasing: Picosecond control of coherent magnetization dynamics in Permalloy thin films by picosecond magnetic field pulse shaping, J. Magn. Magn. Mater. **240**, 283–286 (2002)
29. Th. Gerrits, H. A. M. van den Berg, J. Hohlfeld, L. Bär, Th. Rasing: Ultrafast precessional magnetization reversal by picosecond magnetic field pulse shaping, Nature **418**, 509–512 (2002)
30. Th. Gerrits, H. A. M. van den Berg, J. Hohlfeld, L. Bär, Th. Rasing: Picosecond coherent magnetization reversal by magnetic field pulse shaping, Proc. Intermag Europe 2002, IEEE Trans. Magn. **38**, 2484 (2002)
31. S. Kaka, S. E. Russek: Precessional switching of submicrometer spin-valves, Appl. Phys. Lett. **80** (16), 1958–2960 (2002)
32. H. W. Schumacher, C. Chappert, P. Crozat, R. C. Sousa, P. P. Freitas, J. Miltat, J. Ferré: Precessional magnetization reversal in microscopic spin valve cells, Proc. Intermag Europe 2002, IEEE Trans. Magn. **38**, 2480 (2002)
33. P. Kabos, A. B. Kos, T. J. Silva: Vectorial second-harmonic magneto-optic Kerr effect measurements, J. Appl. Phys. **87**, 5980 (2000)
34. Th. Rasing: Nonlinear magneto-optical probing of magnetic interfaces, Appl. Phys. B **68**, 477–484 (1999)
35. T. M. Crawford, T. J. Silva, C. P. Teplin, C. T. Rogers: Subnanosecond magnetization dynamics measured by the second-harmonic magneto-optic Kerr effect, Appl. Phys. Lett. **74**, 3386 (1999)
36. H. Awano, S. Ohuki, H. Shirai, N. Otha: Magnetic domain expansion readout for amplification of an ultra high density magneto-optical recording signal, Appl. Phys. Lett. **69**, 4257 (1996)
37. H. Awano, M. Sekine, M. Tani, N. Kasajima, N. Otha, K. Mitani, N. Takagi, S. Sumi: 0.04 μm domain expansion readout for the magnetic amplifying magneto-optical system, Jpn. J. Appl. Phys. **39**, 725 (2000)
38. M. Mansuripur: *Physical Principles of Magneto Optical Recording* (Cambridge University Press, Cambridge 1995)
39. H.-P. D. Shieh, M. Kryder: Dynamics and factors controlling regularity of thermomagnetically written domains, J. Appl. Phys. **61**, 1109 (1987)
40. R. Giles, M. Mansuripur: Dynamics of magnetization reversal in amorphous films of rare-earth – transition metal alloys, J. Magn. Soc. Jpn. **15**, Suppl. S1, 299 (1991)
41. M. Hasegawa, K. Moroga, M. Okada, O. Okada, Y. Hidaka: Computer simulation of direct overwrite scheme in the exchange coupled bilayer for magneto-optical memory, J. Magn. Soc. Jpn. **15**, Suppl. S1, 307 (1991)

42. J.F. Herbst, J.J. Croat: Magnetization of R_6Fe_{23} intermetallic compounds: Molecular field theory analysis, J. Appl. Phys. **55**, 3023 (1984)
43. J. Hohlfeld, S.-S. Wellershoff, J. Güdde, U. Conrad, V. Jähnke, E. Matthias: Electron and lattice dynamics following optical excitation of metals, Chem. Phys. **253**, 237 (2000), references therein
44. H.A.M. van den Berg, W. Clemens, G. Gieres, G. Rupp, M. Vieth, J. Wecker, S. Zoll: GMR angle detector with an artificial antiferromagnetic subsystem (AAF) J. Magn. Magn. Mater. **165**, 524 (1997)
45. A. Scholl, L. Baumgarten, R. Jacqemin, W. Eberhardt: Ultrafast spin dynamics of ferromagnetic thin films observed by femtosecond spin-resolved two-photon photoemission, Phys. Rev. Lett. **79**, 5146 (1997)
46. G. Mitrikas, C.C. Trapalis, G. Kordas: Electron spin–lattice relaxation of silver nanoparticles embedded in SiO_2 and TiO_2 matrices, J. Chem. Phys. **111**, 8090 (1999)
47. N.D. Rizzo, T.J. Silva, A.B. Kos: Relaxation times for magnetization reversal in a high coercivity magnetic thin film, Phys. Rev. Lett. **83**, 4876 (1999)
48. T. Katayama, M. Miyazaki, H. Arimune, T. Shibata: Effect of 3RD elements on magnetic and magneto-optical properties in amorphous R–T film, J. Magn. Soc. Jpn. **8**, 121 (1984)